SIGNALING AND CELL PHYSIOLOGY

Physiology and cell biology of acupuncture observed in calcium signaling activated by acoustic shear wave

Geng Li · Jie-Ming Liang · Pei-Wen Li · Xiaoqiang Yao · Peter Zhong Pei · Wei Li · Qi-Hua He · Xifei Yang · Queenie C. C. Chan · Paul Y. S. Cheung · Qi Yuan Ma · Siu Kam Lam · Patrick Y. C. Cheng · Edward S. Yang

Abstract This article presents a novel model of acupuncture physiology based on cellular calcium activation by an acoustic shear wave (ASW) generated by the mechanical movement of the needle. An acupuncture needle was driven by a piezoelectric transducer at 100 Hz or below, and the ASW in human calf was imaged by magnetic resonance elastography. At the cell level, the ASW activated intracellular Ca^{2+} transients and oscillations in fibroblasts and endothelial, ventricular myocytes and neuronal PC-12 cells along with frequency–amplitude tuning and memory capabilities. Monitoring in vivo mammalian experiments with ASW, enhancement of endorphin in blood plasma and blocking by Gd^{3+} were observed; and increased Ca^{2+} fluorescence in mouse hind leg muscle was imaged by two-photon microscopy. In contrast with traditional acupuncture models, the signal source is derived from the total acoustic energy. ASW signaling makes use of the anisotropy of elasticity of

Geng Li and Jie-Ming Liang contributed equally to this work.

G. Li · Q. Y. Ma · E. S. Yang
Time Medical Systems,
No. 2, Science Park West Avenue,
Hong Kong, China

J.-M. Liang
Biomedical Engineering, The University of Hong Kong,
Hong Kong, China

P. Y. S. Cheung · S. K. Lam · P. Y. C. Cheng · E. S. Yang
The University of Hong Kong,
Hong Kong, China

P.-W. Li · E. S. Yang
EE Department, National Central University,
Chungli, Taiwan

X. Yao
School of Biomedical Sciences,
Chinese University of Hong Kong,
Hong Kong, China

P. Z. Pei · W. Li
Department Neurology,
The First Affiliated Hospital of Sun Yat-Sen University,
Guangzhou, China

Q.-H. He
Health Science Center, Peking University,
Beijing, China

X. Yang
Shenzhen Center for Disease Control and Prevention,
Shenzhen, China

Q. C. C. Chan
Philips Electronics HK Ltd,
Science Park,
Hong Kong, China

E. S. Yang (✉)
Columbia University,
New York, NY, USA
e-mail: esyang123@hotmail.com

tissues as its waveguides for transmission and that cell activation is not based on the nervous system.

Keywords Acupuncture · Acoustic wave · MRE · Ca²⁺ ion channel · Human · Mice · Fibroblast · Endothelial cells

Abbreviations
ASW   Acoustic shear wave
MRE   Magnetic resonance elastography

Introduction

Acupuncture (Latin for needle prick) is an ancient Chinese art of healing. Along with it is a system of tracks called meridians by the practitioners but invisible anatomically. The great biochemist-turned-historian Joseph Needham described it intuitively as "a system of channels for transporting energy and fundamentally circulatory in nature to all tissues round the body" [15]. Although this medical practice has been in existence for three millennia, its therapeutic purpose has been considered seriously in the West only in the last 30 years [20]. The pertinent question is whether this art of healing can be turned into science, making the experiments observable, reproducible, and conformable to the current knowledge of physiology and cell biology.

Recently, acupuncture analgesia received strong support from clinical studies in Germany. Randomized large-scale clinical trials have demonstrated its effectiveness in migraine [4, 14], osteoarthritis [23], and chronic knee and back pain [7]. Various techniques have been tried to elucidate the basic mechanism of acupuncture. These include thermal imaging, ultrasound, proton-induced X-ray emission, low resistance path tracing, radioactive tracing, and trigger point correlation among others [20]. Making use of functional magnetic resonance imaging (MRI), activation sites in the brain have been reported in tests with acupuncture [11, 13]. However, the nature of the acupuncture signal and its transmission remain elusive.

Our approach to unravel the complexity of acupuncture was to get down to the most elementary principles. We started by formulating the mechanical movement of the needle of the acupuncturist as an acoustic shear wave (ASW) such that its function is mathematically well defined. The model was tested in human calf muscle and observed by using a method called magnetic resonance elastography (MRE) [16]. In MRI, a standard practice of imaging the slow movement of molecules in blood flow is known as the MR angiography. MRE is based on the same principle except that an ASW is used and the molecules

observed are in tissues and muscles. The acoustic signal is generated by a piezoelectric transducer and coupled to the tissues of interest. A pulse sequence using phase-locked cyclic motion-sensitizing gradients is employed to encode the motion as phases in the MR images. By accumulating phases during several wave cycles, the signal can depict cyclic motions with an amplitude less than 100 nm [16]. Instead of modeling the jerking and irregular motions of the typical needle, we used a sinusoid so that the result and interpretation were simplified. Human subjects were employed.

To observe the cellular response to ASW, cells were put in a Petri dish in a high-viscosity methyl cellulose solution. This special arrangement is necessary to mimic the tissues and provide proper acoustic wave coupling not available with water. An acupuncture needle driven by a piezoelectric element was applied to the gel to produce the ASW. The ASW was imaged by MRE and the activities of the cells were observed under a confocal microscope. Spatial and temporal responses through Ca²⁺ activation were recorded for fibroblast, endothelial, cardiac myocytes, and neuronal PC-12 cells.

To link the calcium activities from cell lines to animals, Ca²⁺ fluorescence was observed in vivo using a two-photon laser imaging technique. Additional support of calcium activation was obtained by measurement of endorphin in blood plasma and Gd³⁺ blocking. The series of experiments were designed to show that the self-consistency of the proposed model has no internal conflicts. No experiment on pain suppression was carried out.

Methods

Mechanical measurement

In studying acupuncture, an important and frequently overlooked procedure is the manual needle manipulation performed by acupuncturists after needle insertion. The needle manipulations are typically a series of rapid bidirectional rotation or up-and-down piston movements. Spatially mapped and quantified by ultrasound, the needle stimulus is visualized to wind the tissue and cause tissue displacements of up to 100 μm [12]. In our experiment, the displacement produced by the moving needle was directly measured and visualized with MRE. MRE with a piezoelectric-driven needle driver [3, 16] was used to observe the generation and transmission of the ASW in clinical acupuncture in human subjects. The acupuncture needle was inserted at the acupoint GB 35 (Fig. 1a) located at the calf muscle and adjacent non-acupoint located 1 cm laterally in a GE 1.5-T scanner. The waves induced by the vibrating needle (Fig. 1b) were
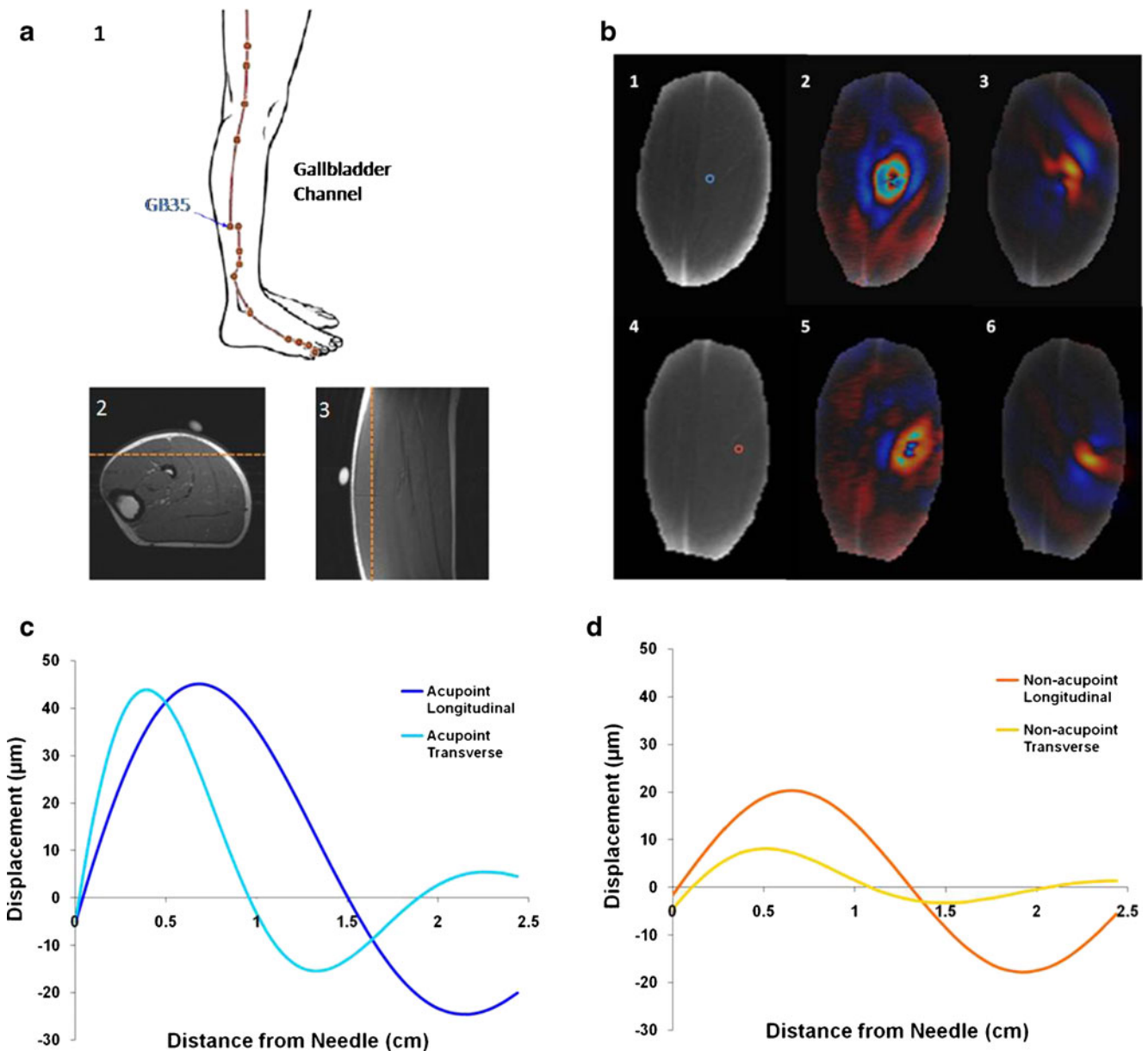
Fig. 1 Study of acupuncture mechanism based on acoustic wave signaling. **a** Location of acupoint GB 35 in the gallbladder channel. T1 images showing the slice orientation of the MRE scan. **b** Coronal T1-weighted images, wave images in transverse direction, and wave images in longitudinal direction with needle at acupoint (*blue open circle, 1–3*), and adjacent non-acupoint (*red open circle, 4–6*). **c** Wave propagation profiles in longitudinal and transverse direction at acupoint. **d** Wave propagation profiles in longitudinal and transverse directions at non-acupoint

measured with a phase-locked motion-sensitizing field gradient echo MR sequence. The direction of the motion-sensitizing field gradients was collinear with the longitudinal motion of the driver and perpendicular to the wave propagation direction. Figure 1c shows an example of the fitted line profile data to damped sinusoid model in the form of $A(x)=A_o \cdot \sin(kx) \cdot \exp(-x/d)$ at the acupoint, where x is the distance away from the needle activation, A_o is the initial amplitude of the field at the needle, k is the wave number equal to $2\pi/\lambda$ and λ is the wavelength, and d is the

delay or attenuation length. The shear stiffness is calculated using Eq. 1 [1, 10] and the anisotropic index was calculated using Eq. 2 [19].

Cell culture

Mouse embryonic fibroblast cell line NIH 3T3 and murine microvascular endothelial cell line H5V were maintained at 37°C in a 5% CO_2 humidified incubator in Dulbecco's modified Eagle's medium (Gibco) supplemented with 10%

fetal bovine serum (Gibco), 100 U/ml penicillin, and 100 μg/ml streptomycin.

Calcium imaging

Cells were grown to 80% confluence prior to calcium imaging. The fluorescent Ca^{2+} indicator dye is Calcium Green-1 for NIH 3T3 and Fluo-4/AM for H5V. The free cytosolic Ca^{2+} concentration in NIH 3T3 and H5V was recorded by the inverted laser-scanning confocal microscope (Olympus FluoView FV1000). Cells were bathed in 2% methyl cellulose solution with Hank's buffered salt solution (Gibco) as basal medium for confocal imaging. The same piezoelectric needle driver was applied to generate acoustic waves in the methyl cellulose medium.

In vivo two-photon calcium imaging

With regard to animal ethics, approval was obtained through Peking/Beijing University (PKU) IACUC for live animal acupuncture studies under approval ID IMM-ChengHP-14. The hind limb muscle of 8-week-old C57BL/6N mice was transfected with GCaMP2 cDNA by electroporation. In brief, 40 μg of expression plasmid was injected, followed by controlled electric pulses (30 V/20 ms duration) delivered by needle electrodes inserted into the skeletal muscle. One to two weeks after transfection, the operated animal was anesthetized, shaved, and mounted for observation. The acupuncture needle was inserted into the hind limb muscle at the acupoint ST36 and the acupuncture needle was driven by a piezoelectric bending element (D220-A4-503YB, Piezo Systems, Inc.) at 1 Hz. A sham acupuncture needle was inserted into the hind limb muscle without any stimulation. Ca^{2+} signal was monitored by the Leica TCS SP5 two-photon laser-scanning microscope system coupled to an upright microscope (CFS, Leica). Two-photon fluorescence images were acquired through a ×20 water immersion objective (HCX, APO, ×1.20/1.00 W, Leica) using 488 nm light for fluorescence excitation (argon laser).

β-Endorphin immunoassay

Four-week-old C57BL/6N mice were kept in a specially designed holder with their hind legs and tails exposed during acupuncture. An acupuncture needle (Hwato) 0.4 mm in diameter and 50 mm in length was inserted into the right hind leg, between the tibia and fibula, approximately 5 mm lateral to the anterior tubercle of the tibia. The acupuncture needle was driven by a piezoelectric bending element (D220-A4-503YB, Piezo Systems, Inc.) at 1 Hz. After receiving acupuncture treatment for 40 min, animals were sacrificed. Blood samples were harvested from the left ventricle of the heart. Plasma was separated by centrifuging samples at 1,000×g for 15 min at 4°C and diluted 1:10 in a sample diluted before assay. The levels of plasma β-endorphin were measured using a mouse β-endorphin ELISA kit from USCN Life Science.

Magnetic resonance elastography

With regard to human ethics, institutional review board approval was obtained through the University of Hong Kong under approval ID #UW04-128T/450. Written informed consent was obtained for all volunteers. Twelve healthy male volunteers aged 24.83±1.95 years, with weight of 63.83±6.81 kg and height of 170.25±7.57 cm, underwent the acupuncture study by MRE [16]. Insertion of the acupuncture needle at the acupoint GB 35 and adjacent non-acupoint during in vivo MRE scans was performed in humans at the right leg. The non-acupoint was located 1 cm lateral to the acupoint GB 35. The needle driver consisted of a piezoelectric bending element (D220-A4-503YB, Piezo Systems, Inc.). The needles (Hwato) were 0.4 mm in diameter, 50 mm long, and made of sterilized pure silver, which were disposed after use. Mechanical excitation was applied at the thigh muscle by the vertical movements of the needle. The MRE study was performed in a 1.5-T MRI scanner (Signa Horizon Echo Speed with version 5.51 software, General Electric Medical Systems, Milwaukee, WI, USA). The waves induced by the needle were measured with a phase-locked motion-sensitized gradient echo MR sequence. Typical data acquisition parameters were TR, 150 ms; TE, 50 ms; flip angle, 30°; acquisition matrix, 256×64; field of view (FOV), 24 cm; and acquisition time, 115.2 s per slice. The frequency of mechanical excitation was fixed at 100 Hz. The number of motion-sensitizing gradients used was 2 at 100 Hz. Six dynamics were obtained by changing the phase offset between the mechanical excitation and the motion-sensitizing gradient to obtain the image of propagation of the shear waves. We define longitudinal as the direction along the muscle fiber and transverse as the direction perpendicular to the muscle fiber.

Phantom experiments

The same needle driver described above was used to generate propagating waves through a 2% methyl cellulose medium (4,000 cPs viscosity, Sigma) in a chamber of 100 mm diameter and 20 mm height. MRE was applied to visualize propagating shear waves. Wave images were obtained on a Philips Intera Achieva 3T system with SENSE Flex-M coil. The FOV was 90 mm with an isotropic voxel size of 1.4 mm in all three directions. The mechanical excitation frequency was 80 Hz. A Piezo-

Acoustic Transducer Model in COMSOL Multiphysics 3.4 (http://www.comsol.com/showroom/gallery/1477/) was used to simulate the acoustic pressure distribution within methyl cellulose solution according to manufacturer's instructions.

Statistical analyses

Statistical data were reported as means±SEM. Significance was tested by analysis of variance or Student's *t* test. A *p* value less than 0.05 was considered statistically significant.

Basic formulae in acoustics

The shear stiffness is calculated using the following equation:

$$\mu = \rho f^2 \lambda^2 \tag{1}$$

where ρ is the density of the material, f is the excitation frequency, and λ is the wavelength determined from the wave images. MRE data were processed using a damped sinusoid model. A line profile was drawn along the wave propagation direction and fitted into the damped sinusoid model to estimate the wavelength. The density ρ is assumed to be 1.1 g/cm^3 for muscle tissue in the literature [5].

Anisotropic index was calculated using the equation:

$$\tau = \mu_{//} - \mu_{\perp} \tag{2}$$

where $\mu_{//}$ is the shear stiffness measured along the muscle fiber direction and $\mu_{\perp}$ is the shear stiffness measured in the perpendicular direction.

Results

Based on the procedure discussed in relation to Fig. 1a–c, we are in a position to study the nature of acoustic wave propagation in the human muscle. The significant difference of the longitudinal and transverse components came from the anisotropy of the muscle elasticity without any reflected waves. The amplitude decayed to a tenth of its initial value in 6.18 and 2.43 cm along the longitudinal and transverse direction, respectively, suggesting the corresponding decay length of 2.684 and 1.055 cm. The fitted line profile of the longitudinal component at non-acupoint is shown in Fig. 1d. The generated signal at the non-acupoint was roughly one half of the amplitude but its wavelength was just slightly less. Thus, it appears that non-acupoint activation could have a similar but reduced effect in comparison with acupoint activation. The anisotropic indices for the acupoint and non-acupoint in the example given in Fig. 1c, d are 2.46 and 1.47 g/cm s^2, respectively.

The measured elasticity values were statistically tested using one-way ANOVA.

A series of experiments focusing on ion channels have been designed to uncover the ASW effect of acupuncture. The experimental setup is shown in Fig. 2a. The acupuncture needle was driven by a piezoelectric driver. It produced the ASW that was applied to the tissue-simulating methyl cellulose medium. The wave then propagated to reach the targeted cells seeded at the bottom. Images were taken by MRE to characterize the wavelength, amplitude, and attenuation of the ASW (Fig. 2b). Acoustic pressure distribution in methyl cellulose was simulated by COMSOL Multiphysics (Fig. 2c). Intracellular signals were monitored and recorded by confocal microscopy.

We first used a mouse embryonic fibroblast cell line (NIH 3T3) as a model. A rise in cytosolic Ca^{2+} was observed following needle driver stimulation. The phase shifts of Ca^{2+} signals in three individual cells (Fig. 2d) show that the Ca^{2+} transient first appears (1) at the upper left corner 0.5 cm from the needle, then spreads towards (2) the center, and finally (3) at the lower right corner. A quantitative analysis of the Ca^{2+} rise times and peak amplitudes are shown in Fig. 2e, f. The normalized peak amplitude of the Ca^{2+} rises also reduced gradually from 0.55 at the source of the acoustic wave (1), through 0.3 at point 2 to 0.15 at the final point 3. The normalized peak amplitude exponentially decays with the distance away from the source of acoustic wave (normalized peak amplitude exp(−x/d)), primarily resulting from the ASW attenuation during propagation. Attendant to the peak amplitude attenuation is the significantly increasing latency for stimulated cytosolic Ca^{2+} rise from 50 through 125 to 325 s. It is noted that the latency and amplitude of the Ca^{2+} transient could be tuned by the local strength of the waves.

A second cell model was murine microvascular endothelial cell line H5V. H5V cells responded to acupuncture-induced acoustic waves by oscillatory rise in cytosolic Ca^{2+}. Figure 3a indicates that responses are extremely heterogeneous in frequency, amplitude, and latency due to the spatial dependence of acoustic wave intensities. The average Ca^{2+} oscillation frequency and peak amplitude decreased modestly as the acoustic wave attenuates with distance (Fig. 3a). In addition, there was a significant change in the latency for Ca^{2+} rise: 4.98±1.01 min at a site 0.5 cm from the needle driver, 14.40±5.19 min at 1 cm, and 32.75±7.23 min at 1.5 cm. Similar to NIH 3T3, gating threshold to elicit cytosolic Ca^{2+} rise in H5V was elevated where the acoustic signal amplitude was small (Fig. 3c). A surprising finding is that the Ca^{2+} oscillation remained at 30 min or even 1.5 h after the needle simulation was turned off (Fig. 3b). The latency and memory effects appeared to be in agreement with the long-lasting healing claimed in traditional acupuncture treatment. Fixing the driver voltage
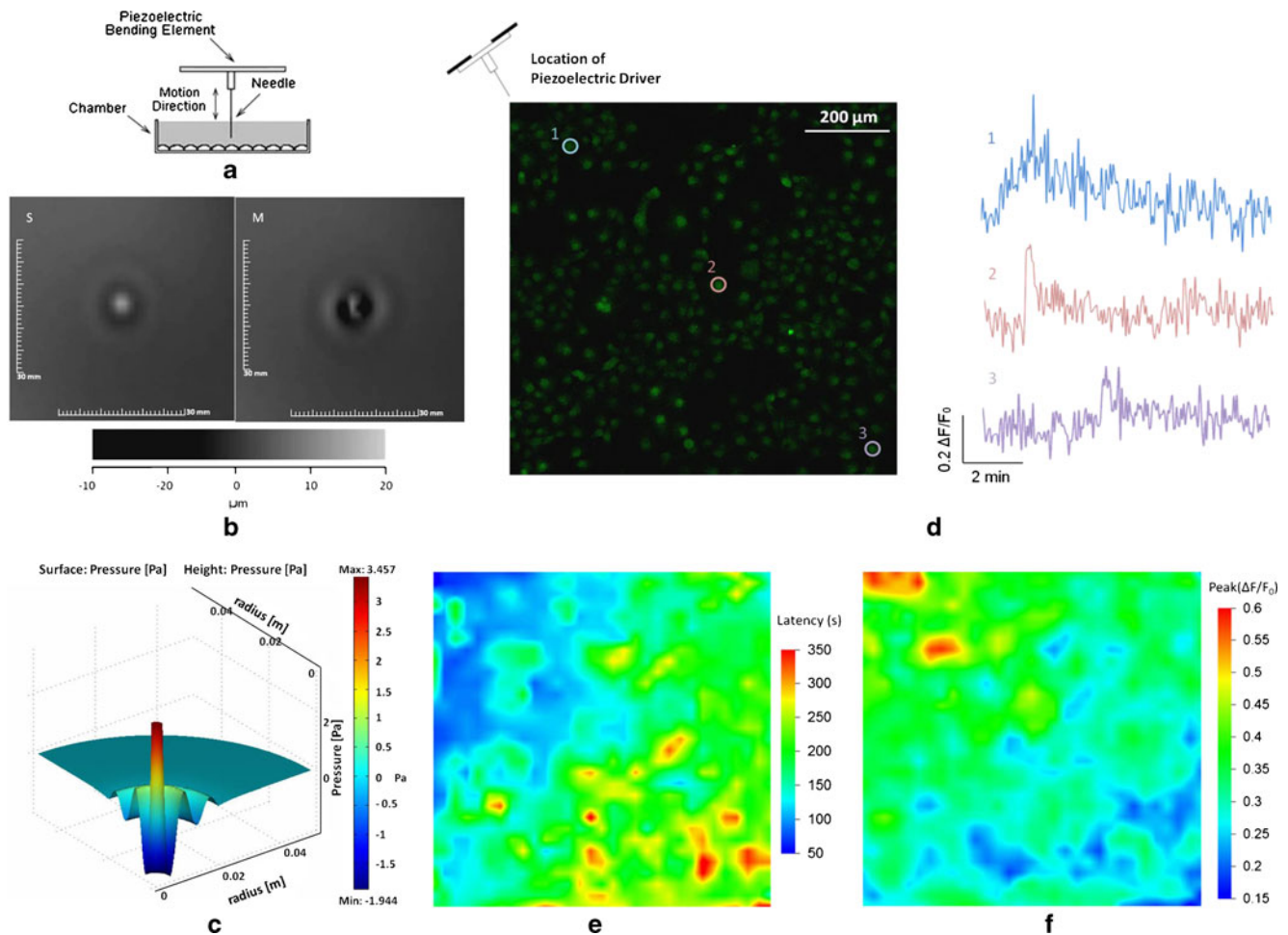
Fig. 2 Ca^{2+} excitation in fibroblast (NIH 3T3) by acupuncture-induced acoustic waves. **a** Piezoelectric driver to provide vertical motion of the needle inside methyl cellulose solution. **b** MRE wave images generated by the needle shear wave driver. **c** Simulated acoustic pressure distribution of methyl cellulose solution. COMSOL Multiphysics 3.4 was used to simulate the coupling of the needle shear wave to methyl cellulose. The maximum acoustic pressure is 3.457 Pa at the center. **d** Confocal microscopy image of Calcium Green-1-loaded NIH 3T3 cells under a ×10 objective lens. Peak Ca^{2+} transient spread from cells at the *upper left* then propagate to neighboring cells seconds later. **e** The 3D color-coded map shows the spatial distribution of latency of propagating Ca^{2+}. The latency mesh is taken as the average of six individual experiments. **f** A 3D contour plot shows the spatial distribution of normalized peak amplitudes of Ca^{2+} transients. The amplitude mesh is taken as the average of six individual experiments. The product of the peak amplitude square and the latency is calculated to be constant of ~13 at points 1 ($0.52 \times 0.52 \times 45 = 12.2$), 2 ($0.35 \times 0.35 \times 100 = 12.3$), and 3 ($0.23 \times 0.23 \times 230 = 12.1$)

of the piezoelectric element, the frequency response of the amplitude decreases linearly in Fig. 3d.

Ca^{2+} activation evoked by acupuncture-induced acoustic waves was also present in cells originating from different tissues including ventricular myocytes and PC-12, as shown in Fig. 4. Since both excitable and non-excitable cells were activated by ASW, it might be a fundamental cellular property. Thus, this study provides new insight with a better understanding of acupuncture's effectiveness. To further understand the cellular basis of acupuncture needling, we have made additional studies of the Ca^{2+} channels involved in ASW response and found the following: (1) Acupuncture needle stimulation induced Ca^{2+} excitation in NIH 3T3 and H5V, but failed to elicit Ca^{2+} in the cells treated with Ca^{2+}-free, 5-mM ethylene glycol tetraacetic acid buffer; (2) the application of 100 μM Gd^{3+}, a non-specific mechanosensitive Ca^{2+} channel blocker, completely abolished the channel activity; and (3) 200-μM streptomycin, another blocker for mechanosensitive Ca^{2+} channels, also inhibited the Ca^{2+} rise.

In vivo experiments were carried out on 8-week-old C57BL/6N mice. The mouse's hind limb muscle was transfected with GCaMP2 cDNA by electroporation. Two weeks after transfection, the animal was anesthetized, shaved, mounted, and acupuncture needle was inserted into the hind limb muscle at acupoint ST36. Ca^{2+} level was monitored by two-photon confocal microscopy. ASW induced a robust and significant increase in fluorescence in hind limb muscle fiber at the site of stimulation and the ASW-
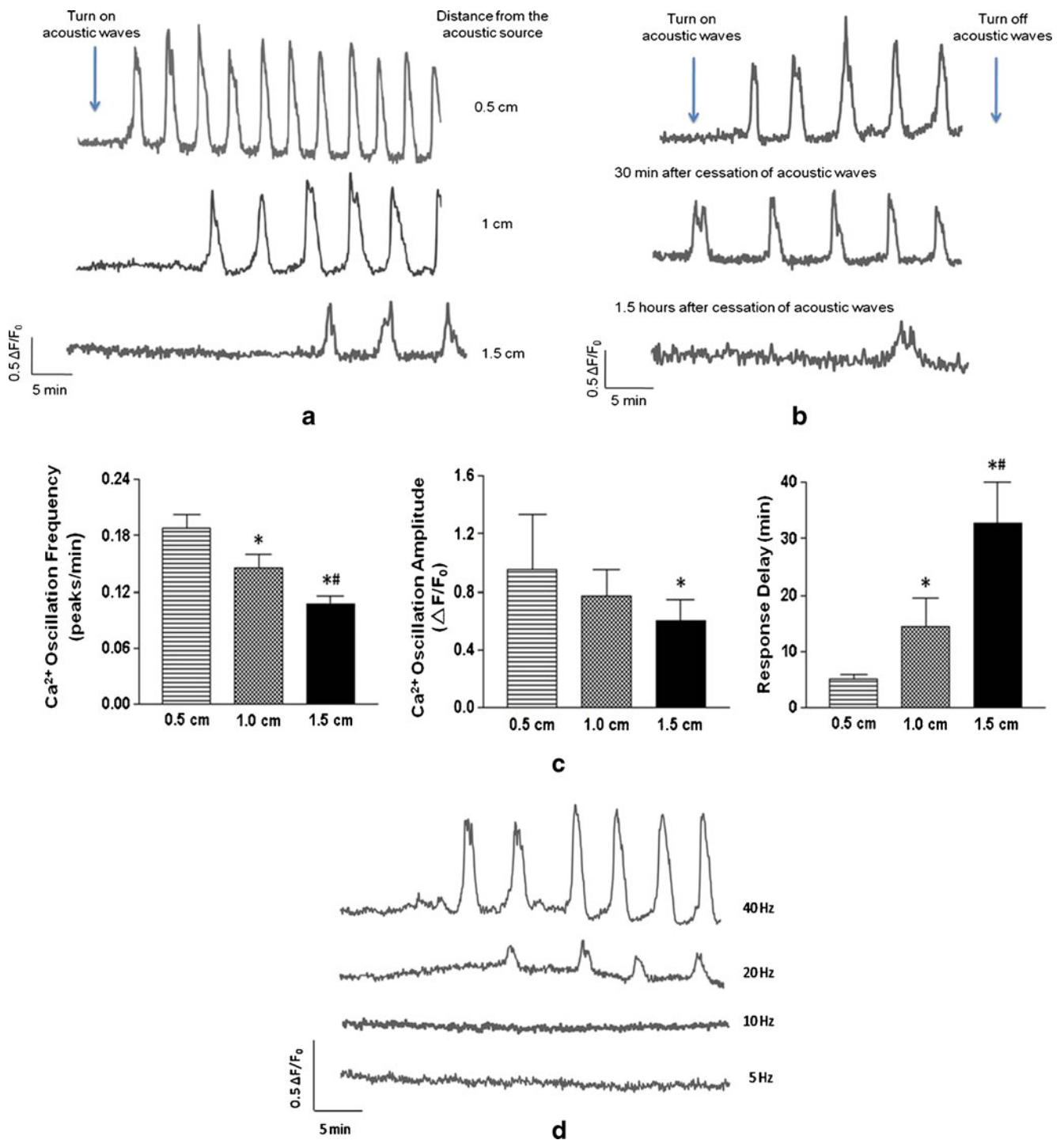
Fig. 3 Ca^{2+} oscillations when endothelial H5V cells are exposed to ASW propagating in high-viscosity methyl cellulose solution. **a** Three typical profiles of single-cell Ca^{2+} recording. **b** Memory effects of H5V. **c** Statistical analysis of the dose-dependent effect of single-cell Ca^{2+} oscillations. The Ca^{2+} oscillation frequency and peak Ca^{2+} amplitude decrease as the acoustic wave attenuates with distance (0.5,

1, and 1.5 cm from the acoustic source, $n=8\times3=24$). And the single-cell Ca^{2+} response delay increases as the acoustic wave diminishes in the medium. $*p<0.05$, significant versus the 0.5-cm group; $\#p<0.05$, significant versus the 1-cm group. **d** Response of H5V subjected to acoustic wave of different frequencies; region of interest around 0.5 cm away from the needle driver driven by a constant voltage

induced fluorescence signal was subsequently propagated to the adjacent muscle fibers, suggesting an acupuncture-stimulated Ca^{2+} response (Fig. 5a, b). The light emission

enhancement is similar to that of Ca^{2+} uptake into the mitochondria of the mouse's hind limb muscle upon tetanic contraction [18].
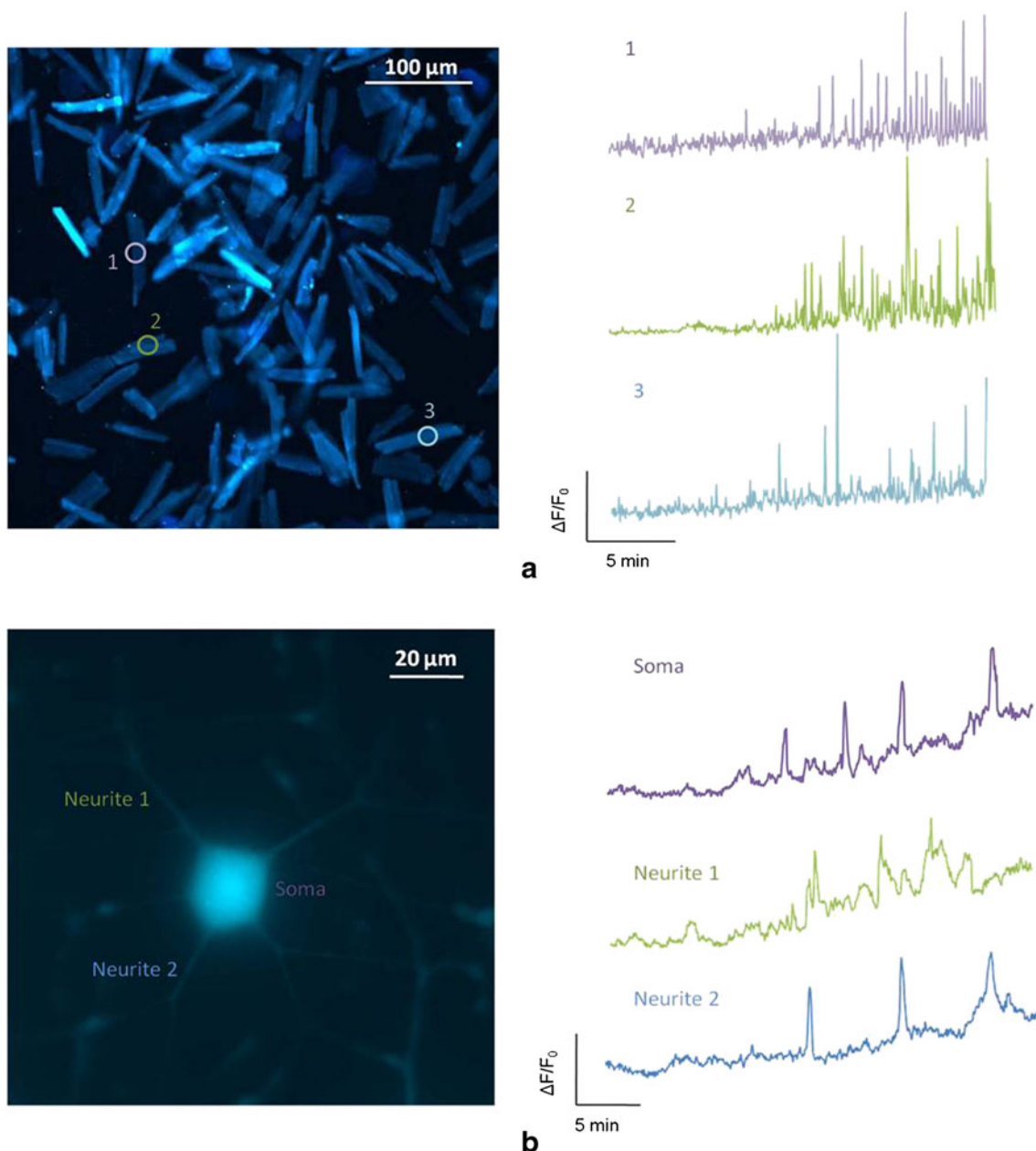
Fig. 4 Ca^{2+} excitation of rat ventricular myocytes and differentiated PC-12 in response to acupuncture-induced acoustic waves. **a** Confocal microscopy image of Fura-2/AM-loaded ventricular myocytes under a ×20 objective lens. Acoustic waves are turned on within 1 min upon recording. Contraction pulses and increase of Ca^{2+} transients are detected after a certain period of delay. **b** Confocal microscopy image of Fura-2/AM-loaded differentiated PC-12 under a ×60 objective lens. Ca^{2+} oscillations of differentiated PC-12 are detected when exposed to acoustic waves

In the second in vivo experiment, acupuncture was initiated by the needle driver described above in the hind limb muscle of the mouse. Plasma β-endorphin was measured 40 min after the acupuncture treatment by immunoassay. Elevation of β-endorphin levels was observed (Fig. 5c) along with cytosolic Ca^{2+} activation in muscle fibers in vivo 40 min after the stimulation was applied. The acupuncture-induced β-endorphin increase was blocked by the intraperitoneal injection of Gd^{3+}, an inhibitor for mechanosensitive Ca^{2+} channels. It is possible that acupuncture-induced Ca^{2+} signaling may contribute to β-endorphin release.

Discussion

In acupuncture, the signal is broadcasted with the wave radiating from the needle like a radio antenna. The muscle, being a fiber bundle, is an anisotropic medium for sound as

Fig. 5 In vivo Ca^{2+} signals induced by acupuncture in mouse skeletal muscle. **a** Transfected muscle fibers exhibited weak GCaMP2 fluorescence in vivo without ASW. **b** Enhanced brightness in fluorescence signal of GCaMP2 observed under ASW stimulation indicates cytosolic Ca^{2+} was excited by acupuncture. **c** Gd^{3+} completely reversed acupuncture-induced increase in plasma β-endorphin of the mice. *Error bars* represent SEM; $n=4$; *$p<0.05$ versus the acupuncture-treated group
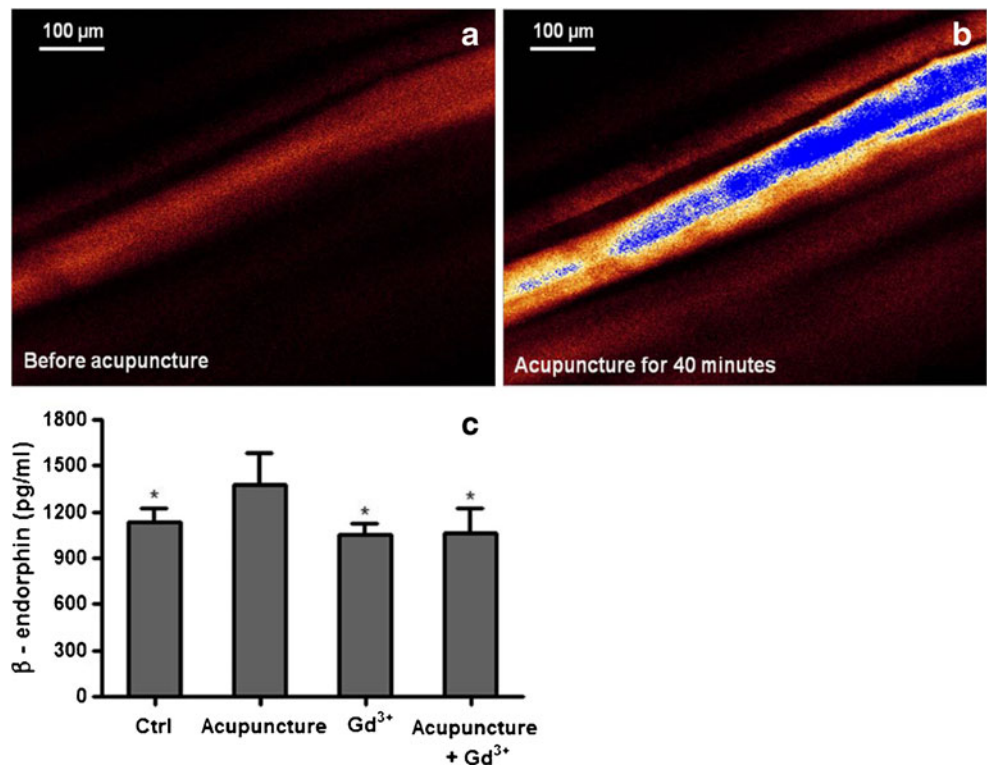
observed in wave propagation through the biceps brachii muscle with a chevron-like pattern [5]. With low absorption coefficient at low frequency, the attenuation is small so that the acoustic wave can easily reach the cells or nerve endings. In addition, the elasticity of the muscle in the relaxed and contracted state can differ by more than a 100-fold [6], and an 8-fold increase has been detected in MRE [5]. The insertion of a needle tends to contract a muscle, increasing the anisotropy and reducing the attenuation. These physical properties made the muscle an effective but somewhat leaky acoustic waveguide. As in any waveguide, symmetry is important for wave propagation. In a muscle, the acupoint and non-acupoint did not induce the same tissue displacement. With the same applied voltage to the piezoelectric transducer, the acoustic wave amplitude at the acupoint and the sham point differed by a factor of ~2.5, as shown in Fig. 1c, d. As pointed out previously, the connective tissue network may play a key role in the transmission of the mechanical needling process of cellular events [12]. The acupoint and sham point, being laterally separated by 1 cm, are likely to engage different collagen fibers, producing different mechanical coupling. Thus, the importance of stress guiding and anatomical distinction between acupoint and sham point cannot be underestimated. This phenomenon would explain a significant contrast in producing the acupuncture signal and its pathway.

Although there was a substantial difference between the responses of the acupoint and sham point, both could produce a measurable ASW that could reach the cell levels. It would also depend on the anatomical location of the points of activation. Our experimental finding is that the coupling or energy transfer at the acupoint and sham point appears to produce the difference in signal amplitude, and the cell latency primarily relates to the attenuated acoustic signal of which the cell is sensitive (Fig. 2). We also discovered that there appears to be a constant value for the product of the peak amplitude square and the latency ($A_o^2 \times$ latency=constant), suggesting a threshold acoustic energy required for activating the cell. Further support for this line of reasoning is evidenced by the experimental observations (Fig. 3d) that the peak amplitude square has an inverse dependence on the applied acoustic signal frequency (between 10 and 80 Hz), indicating that the acupuncture is actually independent of the applied signal frequency, but strictly follows the acoustic energy. This would also explain why some of the clinical trials, e.g., in migraine, knee and back pain studies, showed that both methods were effective [4, 7, 14, 23]. It is also consistent with the observation that the traditional acupoint activation was, in most cases, better than the sham acupuncture [4, 23]. In practice, the clinician does not have to hit the bull's eye and deviation from acupoints is acceptable.

As for the mechanotransduction, we observed that the ASW is able to produce cytosolic Ca^{2+} oscillations in endothelial cells similar to that produced by a Ca^{2+}-mobilizing agonist histamine [9] (Fig. 3a). It is significant

that there is no involvement of action potential or electrical excitation and that only a change in cytosolic Ca^{2+} is involved. In the literature, it is widely believed that Ca^{2+} oscillations can serve as second messenger [2, 22]. The memory effect seen in Fig. 3b can be explained by having the endoplasmic reticulum as the Ca^{2+} stores and its buildup and release could produce the regenerative oscillation. This is, however, speculative and requires more study [8, 17]. In our data, the surprisingly long-lasting Ca^{2+} oscillations seen after an hour of actuation are testimonies of the power of acupuncture in migrant headache in which healing is now recognized more effective than a chemical drug and yet without side effects.

Another significant point in our study is the result of in vivo two-photon microscopy with ASW. Previously, it was demonstrated that both cytoplasmic and mitochondrial Ca^{2+} transients can be monitored using the genetically encoded fluorescent calcium indicator protein GCaMP2 [21]. In vivo and under highly physiological conditions, mitochondria in mouse skeletal muscle take up Ca^{2+} during contraction and rapidly release it during relaxation. The rise in Ca^{2+} observed during single twitches and tetanic stimulation in live mammalian skeletal muscle is synchronized with the physiological induction of muscle contraction [18]. Instead of inducing contraction by motor nerve stimulation, we have found that the ASW is capable of duplicating the same function. The enhancement of endorphin release and its inhibition by Gd^{3+} with the in vivo mouse study demonstrated the central role of Ca^{2+}. Without ASW, there was no increase in cytosolic Ca^{2+} or endorphin. ASW produced an endorphin increase, which was blocked by Gd^{3+}. Thus, it appears that acupuncture may play the role as the trigger making possible pain relief. Different from other modes of mechanical stimuli, ASW is long-range and dynamic. Thus, latency, memory, Ca^{2+} wave, and accumulative effect can be readily explained in ASW. It should be pointed out that, although the therapeutic effect can be modeled with ASW, our results only suggest a plausible self-consistent mechanism. More experiments are needed to confirm conclusively the effect of analgesia or pain suppression.

Conclusion

Modern imaging and cell biology techniques have been employed to study the nature of acupuncture. By using a vibrating acupuncture needle with a displacement in the range of 100 μm, we have been able to demonstrate that the ancient healing technique can be modeled by the ASW. The ASW, being a mechanical energy, is capable of mechanotransduction, stimulating cytosolic Ca^{2+} rise in both excitable and non-excitable cells, producing Ca^{2+} oscillations, memory, and giving rise to in vivo calcium fluorescence and endorphin release into blood plasma in mice. The mechanism obeys the wave equations and the laws of cell biology so that acupuncture is unencumbered by the mystery of the celestial lancets and its unfathomable ramifications.

References

1. Auld BA (1990) Acoustic fields and waves in solid. Krieger, Melbourne
2. Berridge MJ, Irvine RF (1989) Inositol phosphates and cell signalling. Nature 341:197–205
3. Chan QCC, Li G, Ehman RL, Grimm RC, Li R, Yang ES (2006) Needle shear wave driver for magnetic resonance elastography. Magn Reson Med 55:1175–1179
4. Diener HC et al (2006) Efficacy of acupuncture for the prophylaxis of migraine: a multicentre randomized controlled clinical trial. Lancet Neurol 5:310–316
5. Dresner MA et al (2001) Magnetic resonance elastography of skeletal muscle. J Magn Reson Imaging 13:269–276
6. Duck FA (1990) Physical properties of tissue: a comprehensive reference book. Academic, London
7. Endres HG et al (2007) Acupuncture for the treatment of chronic knee and back pain. Dtsch Arztebl 104:A123–A130
8. Falcke M (2004) Reading the patterns in living cells—the physics of Ca^{2+} signaling. Adv Phys 53:255–440
9. Jacob R et al (1988) Repetitive spikes in cytoplasmic calcium evoked by histamine in human endothelial cells. Nature 335:40–45
10. Kinsler LE, Frey AR, Coppens AB, Sanders JV (1990) Fundamentals of acoustics. Wiley, New York
11. Kong J et al (2007) Test–retest study of fMRI signal change evoked by electroacupuncture stimulation. NeuroImage 34:171–1181
12. Langevin HM et al (2004) Tissue displacements during acupuncture using ultrasound elastography techniques. Ultrasound Med Biol 30:1173–1183
13. Li G et al (2006) An fMRI study of somatosensory-implicated acupuncture points in stable somatosensory stroke patients. J Magn Reson Imaging 24:1018–1024
14. Linde K et al (2005) Acupuncture for patients with migraine. JAMA 293:2118–2125

15. Lu GD, Needham J (1980) Celestial lancets: a history and rationale of acupuncture and moxibustion. Cambridge University Press, Cambridge, UK

16. Muthupillai R et al (1995) Magnetic resonance elastography by direct visualization of propagating acoustic strain waves. Science 269(5232):1854–1857

17. Politi A, Gaspers LD, Thomas AP, Hofer T (2006) Models of IP3 and Ca^{2+} oscillations: frequency encoding and identification of underlying feedback. Biophys J 90:3120–3133

18. Rudolf R et al (2004) In vivo monitoring of Ca^{2+} uptake into mitochondria of mouse skeletal muscle during contraction. J Cell Biol 166:527–536

19. Sinkus R et al (2005) Imaging anisotropic and viscous properties of breast tissue by magnetic resonance elastography. Magn Reson Med 53:273–287

20. Stux G, Berman B, Pomeranz B (2003) Basics of acupuncture. Springer, Berlin

21. Tallini YN et al (2006) Imaging cellular signals in the heart in vivo: cardiac expression of the high-signal Ca^{2+} indicator GCaMP2. Proc Natl Acad Sci USA 103:4753–4758

22. Tsien RW, Tsien RY (1990) Calcium channels, stores and oscillations. Annu Rev Cell Biol 6:715–7602

23. Witt C et al (2005) Acupuncture in patients with osteoarthritis of the knee: a randomized trial. Lancet 366:136–143